Journal of Computational Electronics (2022) 21:834–840
https://doi.org/10.1007/s10825-022-01899-5

High-performance surface plasmon resonance-based photonic crystal fiber sensor with four open surface rings

Ali-Porghoveh Neda[1] · Barvestani Jamal[1] · Meshginqalam Bahar[1]

Received: 6 December 2021 / Accepted: 2 May 2022 / Published online: 17 June 2022

Abstract
In this paper, a photonic crystal fiber sensor is proposed with four open-ring channels that enhances sensor performance with increased coupling features. By detecting the optical spectrum of leakage from the fiber core to the channels, the sensitivity of the sensor can be assessed. Gold is used as the plasmonic material coated on titanium oxide film which is employed as a substrate layer to increase adhesion and sensor performance. The influence of structural parameters on the sensor performance is investigated by the finite-difference time-domain method. Sensor response is investigated for a wide refractive index range of 1.34–1.44. As a result of applying these four analyte channels, maximum wavelength and amplitude sensitivity of 25,600 nm/RIU and 7367 RIU^{-1} and figure of merit (FOM) of 547 RIU^{-1}, where RIU is the refractive index unit, were calculated. In addition to high sensitivity, the proper FOM value of this sensor is an important feature which makes it suitable for identifying chemicals and biomolecules.

Keywords Photonic crystal fiber sensor · Surface plasmon resonance · Amplitude sensitivity · Refractive index · Figure of merit

1 Introduction

With the increasing demand for optical sensors, especially for medical applications, as well as the implementation of sensors within integrated circuits, downsizing and increasing the sensitivity of sensors in small dimensions has become very important [1, 2]. One of the sensing mechanisms in the identification of chemicals and biomolecules is the refractive index (RI)-based sensor [2]. In this regard, optical fiber sensors have been designed and fabricated by methods such as Bragg interferometry and grating to monitor water pollution, detect chemicals, and so on [3, 4]. In the last two decades, surface plasmon resonance (SPR) has been used in the development of unlabeled optical sensors with high sensitivity [5]. Surface plasmon amplification takes place when an optical electric field with transverse magnetic wave (TM) polarization is coupled with collective electron oscillation at the boundary between a dielectric and a metal surface. Various studies have explored the application of SPR-based optical sensors using different structures and methods. To date, different SPR-based optical fiber sensors such as conventional fibers [6], Bragg-grating-based fibers [7], photonic quasi-crystal fibers (PQFs) [8] and photonic crystal fibers (PCFs) [9] have been reported. In order to realize system miniaturization and integration, SPR-based PCF sensors (PCF-SPR) have been widely investigated. As a kind of micro-structured optical fiber, PCF presents advantages such as tunable effective RI, large mode area and birefringence [10]. SPR-based PCF sensors offer sensitivity almost twice that of conventional SPR-based fiber sensors [11, 12]. In this regard, various PCF-SPR sensors have been designed and studied. In 2019, Paul et al. proposed a dual-core PCF fiber based on SPR [13]. Two different works report sensitivity of 4850 (nm/RIU) and 5200 (nm/RIU) , where RIU is the RI unit, for D-shaped PCF-SPR sensors [14, 15]. Previously, a three-hole sensor structure was reported by Hautakorpi et al. by tuning the thickness of the dielectric layer [16]. Recently, Momtaj et al. proposed a dual-core PCF-SPR sensor with an open-channel D-shaped structure [17]. In 2021, another open-channel dual-core biosensor was reported for the analyte RI range of 1.33 to 1.45 [18].

To achieve high-performance PCF-SPR sensors, surface engineering of the structure has a vital role. In this work, a

✉ Meshginqalam Bahar
bahar.meshginqalam@tabrizu.ac.ir

[1] Faculty of Physics, University of Tabriz, Tabriz, Iran

novel PCF-SPR sensor with four open-ring surface channels is proposed. These channels are engineered with proper diameter and core-to-channel distance to improve the sensing behavior. Gold is chosen as the plasmonic material due to its low loss and is deposited on theTiO_2 layer to enhance the sensitivity and adhesion. We have numerically reported the sensing characteristics of the proposed PCF sensor by optimizing the structural parameters such as position and radius of surface rings, first air hole radius and thicknesses of gold and TiO_2 films. The results show high values of wavelength and amplitude sensitivity and figure of merit (FOM), making the sensor suitable for various applications.

2 Design and method

A schematic diagram of the proposed PCF-SPR sensor is demonstrated in Fig. 1, where four open-ring channels are created on the surface of the structure which are coated by TiO_2 and gold films. Three hexagonal rows of air holes are stacked in which some rotations have been done, and four holes of the second row are removed to obtain good coupling between the fundamental core and SPR modes appearing at the surface of the four open rings. The radii of holes of the second and third rows are assumed to be $r_2 = r_3 = 0.65$ µm. The distance from the center of the first ring of air holes to the core, pitch (Λ), is fixed to 2 µm. Another two pitches were fixed to 1.4 Λ and 1.8 Λ for the distance of the second and third rings to the core, respectively. These four large open-ring channels are more conducive to the deposition of metal thin films which support SPR modes. The optimized parameters for the four open-ring channels are determined as 1 µm and $R_H = 4$ µm for the radius of rings and the distance from their center to the center of the fiber, respectively. Gold and TiO_2 layers with thicknesses of t_{Au} and t_{TiO_2} are deposited at the inner surface of the open rings.

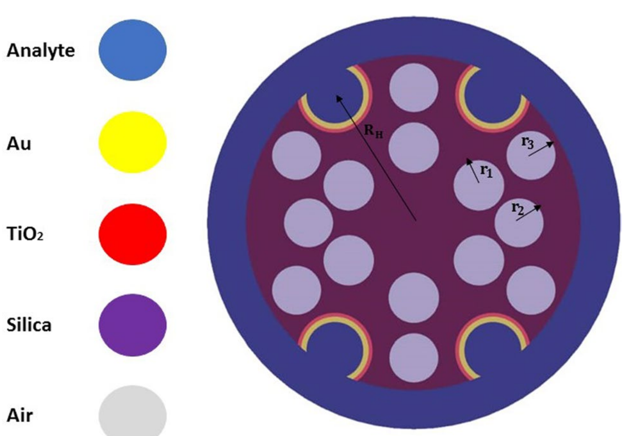

Fig. 1 Two-dimensional cross-sectional view of the proposed PCF sensor with $R_H = 4$ µm, $r_2 = r_3 = 0.65$ µm

Fused silica is selected as the background material for the sensor, and its RI is given by the Sellmeier relation [19]:

$$n^2(\lambda) = 1 + \frac{B_1\lambda^2}{\lambda^2 - C_1} + \frac{B_2\lambda^2}{\lambda^2 - C_2} + \frac{B_3\lambda^2}{\lambda^2 - C_3} \tag{1}$$

where B_1, B_2, B_3, C_1, C_2, and C_3 are known as the Sellmeier constants. The values of these constants for the fused silica are 0.69616300, 0.407942600, 0.897479400, 0.00467914826 µm^2, 0.0135120631 µm^2 and 97.9340025 µm^2, respectively. The permittivity of gold is given by the Drude–Lorenz model [20]. A thin layer of TiO_2 is also used between the gold and silica, which assists in reducing the adhesion problem of Au and improves the sensitivity by enhancing the coupling of the core-guided mode and SPR mode [21]. The dielectric constant of titanium oxide is calculated by the following equation [22]:

$$n^2_{TiO_2}(\lambda) = 5.913 + \frac{2.441 \times 10^7}{\lambda^2 - 0.803 \times 10^7} \tag{2}$$

where λ is the wavelength measured in µm.

The confinement loss is a crucially important performance parameter for the PCF-SPR sensor, which can be determined by the following equation [23]:

$$\alpha(\lambda) = 8.686 \times k_0 \times \mathrm{Im}\left(n_{eff}\right) \times 10^4 \left(\frac{dB}{cm}\right) \tag{3}$$

where the imaginary effective mode index is denoted as $\mathrm{Im}(n_{eff})$, $k_0 = \frac{2\pi}{\lambda}$ is the wave number and λ is the operating wavelength. Analyte sensing happens with the variation of the RI in the surrounding environment for the bio-targets. This is done by measuring the spectral peak displacement and the spectral sensitivity of the PCF sensor S_w is expressed as [24]:

$$S_w = \frac{\Delta\lambda_{peak}}{\Delta n_a}(nm/RIU) \tag{4}$$

Another performance parameter is the amplitude sensitivity, which can be analyzed through the following formula [24]:

$$S_A = -\frac{1}{\alpha\left(\lambda, n_a\right)} \frac{\partial\alpha\left(\lambda, n_a\right)}{\partial n_a}\left(RIU^{-1}\right) \tag{5}$$

where $\alpha(\lambda, n_a)$ shows the confinement loss for wavelength λ and analyte RI of n_a, and $\partial\alpha(\lambda, n_a)$ represents the difference between α values of two adjacent n_a. The resolution of the biosensor can be improved by reducing the full-width at half-maximum (FWHM). The FOM, which provides both sensitivity and FWHM, can be calculated by [25]:

$$FOM = \frac{S_w}{FWHM}\left(RIU^{-1}\right) \quad (6)$$

The simulation and analytical evaluation are conducted by Lumerical software, which uses the finite-difference time-domain (FDTD) method in the presence of a perfectly matched layer to minimize radiation absorption towards the surface.

3 Surface plasmon resonance explanation

This section discusses the significance of surface plasmon resonance with respect to the SPR-based PCF sensors. Plasmons that form at the interface of a metal and dielectric are called surface plasmons (SPs) and can be excited by visible or ultraviolet photons, a phenomenon called surface plasmon resonance [26]. For the case of simple flat metal–dielectric interfaces, a prism with a high dielectric constant is used to obtain the evanescent wave for the excitation of SPs. The resonance phenomenon occurs when the propagation constant of the SP matches the wave vector of the evanescent wave. The satisfied SP modes are guided at the interface of the metal and dielectric and can be excited by photons with the same polarization state as that of SPs. This matching condition causes the energy transfer from photons to SPs, which is dependent on the RI of the dielectrics (analyte). However, in the case of optical fiber SPR sensors, due to the total internal reflection of the core-guided mode, the evanescent wave is presented at the interface of the core and cladding regions. Therefore, the prism is replaced by the fiber core in the case of fiber sensors. The coupling of the evanescent field located at the metal-sensing layer interface and the SP wave strongly depends on the wavelength, fiber geometrical parameters and the metal layer properties. In fact, the phase-matching condition can be satisfied at the intersection point of the effective mode index of the core and the SPR modes. At the resonance wavelengths, the real part of the effective RI of the fiber core and the SPs are equal [27].

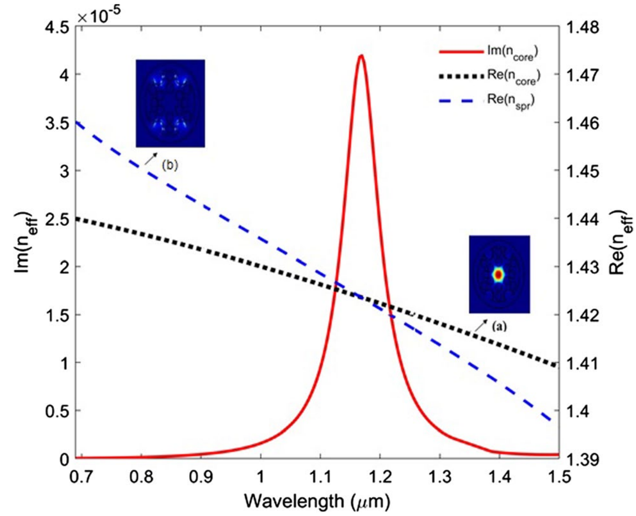

Fig. 2 Dispersion of the fundamental and SPR-guided modes. Dotted and solid curves show the dispersion of the real and imaginary parts of the fundamental mode, respectively, and the dashed curve shows the dispersion of the SPR mode. Inset *a* (*b*) displays the profile of the electric fields for the fundamental core (SPR) mode denoted by an arrow for an analyte RI of 1.43, where $t_{Au} = 40$ nm and $r_1 = 0.67$ µm

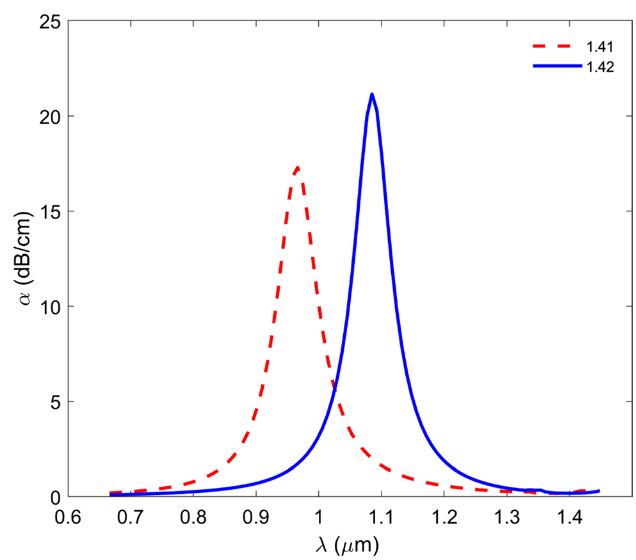

Fig. 3 Loss spectra of proposed sensor for two analyte RIs of 1.41 and 1.42, where t_{TiO_2} = 12nm, $t_{Au} = 40$ nm and $r_1 = 0.65$ µm

4 Results and discussion

This section presents numerical results for the proposed SPR-based PCF sensor for different parameters of the structure. Figure 2 shows the dispersion of fundamental core and SPR modes supported at the surface of rings for the analyte RI of 1.43. The dotted (solid) line shows the dispersion of the real (imaginary) part of the effective RI $\left(n_{eff}\right)$ of the fundamental core mode. In addition, the real part of $\left(n_{eff}\right)$ for the SPR mode is illustrated by the dashed line. By satisfying the phase-matching condition, the core and the plasmonic modes are coupled and a peak is observed in the loss spectra. Thus, this loss peak is related to the intersection point of the real parts of $\left(n_{eff}\right)$ for the core and SPR modes. An unknown sample with a specific RI can be effectively detected by the variation in the corresponding resonance wavelength to a longer or shorter wavelength.

To analyze the sensor performance, firstly, the loss peaks for two analytes with RI of 1.41 and 1.42 are shown in Fig. 3. For the case of 1.41, the loss peak occurred at a wavelength of 0.966 µm, and correspondingly for the case of 1.42, it occurred at 1.085 µm. Thus, according to Eq. (4), the wavelength shift between the two analytes shows a wavelength sensitivity of 11,900 nm/RIU.

In order to investigate the effect of numerous structural parameters on sensor performance and to select the optimized values, all of the parameters are classified and explained in the following figures and tables. These calculations are performed considering analyte RI variations in the range of 1.34–1.44.

To investigate the effects of TiO_2 thickness on the performance of the proposed sensor, we show the sensitivity and FOM values versus the thickness of the TiO_2 film in Fig. 4, in which the gold thickness is fixed at 30 nm and $r_1 = 0.6$ µm. These results show that the highest wavelength sensitivity and FOM values can be obtained as 23,000 (nm/RIU) and 466.66 RIU^{-1} which take place at $t_{TiO_2} = 11$ nm. Thus, we assume $t_{TiO_2} = 11$ nm as an optimum value in the remainder of the paper. Also, we deduce from these data that the presence of the TiO_2 layer has a positive effect on FOM values, while the sensitivity enhancement occurs at greater thicknesses.

Similarly, in Fig. 5, the sensor performance in terms of sensitivity and FOM is plotted for different Au thicknesses.

As is clear from Fig. 5, the maximum values of wavelength sensitivity and FOM relate to the $t_{Au} = 40$ nm. Thus, we choose this value as an optimum value for the proposed sensor in the following. It should be mentioned that the corresponding values are 21,700 (nm/RIU) and 391.66 RIU^{-1}, respectively. Finally, in Fig. 6, the sensor performance using the previous optimum parameters are examined for different r_1 values. As seen from this figure and with respect to the maximum values of the sensitivity and FOM, $r_1 = 0.67$ µm is the optimum value. It worth mentioning that we examine the effect of the sizes of r_2, r_3 and r_H parameters on the performance of the proposed sensor. Our calculated results show that the variations in the rod size of r_2 and r_3 have no significant effect on the sensitivity. Also, the proposed structure showed no uniform or proper peaks for the other values of r_H. Thus, we set the values of these parameters to $r_2 = r_3 = 0.65$ µm and $R_H = 4$ µm throughout the manuscript.

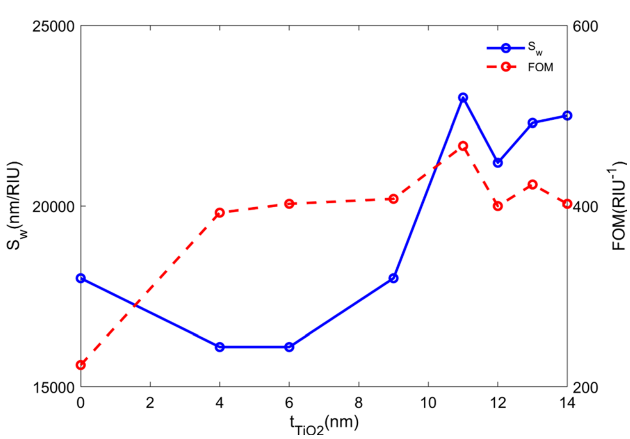

Fig. 4 Calculated wavelength sensitivity and FOM values of proposed sensor versus the thickness of the TiO_2 layer

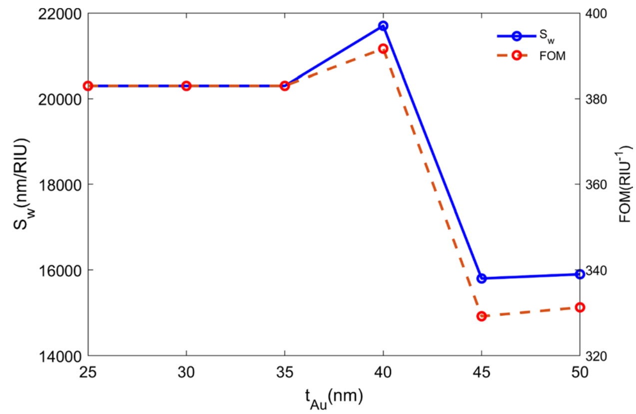

Fig. 5 Calculated wavelength sensitivity and FOM values versus thickness of the gold layer

Now, we plot the loss spectra of the proposed PCF-SPR sensor for various analyte RIs by using optimized values of structural parameters. Loss spectra are presented in Fig. 7 for a wide range of analyte RIs.

The loss peaks have red shifts, and we can conclude that the proposed sensor depicts good sensitivity at higher RIs. To gain better insight, we show corresponding amplitude sensitivity values in Fig. 8. We see that the proposed sensor shows amplitude sensitivity for a wide range of analyte RIs.

It is evident from the figure that the amplitude sensitivity increases gradually with an increase in analyte RI and reaches the maximum value for an analyte RI of 1.43 which is 7367 RIU^{-1}.

To quantitatively show these behaviors, we summarize the corresponding sensing parameters in Table 1.

Finally, to show the performance of the proposed sensor, FOM is plotted versus the analyte RI variations in Fig. 9.

As the RI of the analyte increases, the loss curve becomes sharper. This type of change indicates a decrease in FWHM, which results in an increase in FOM. We obtain the maximum FOM as 547 RIU^{-1} for the case of RI = 1.43.

We comprehensively compare the sensing characteristics of our proposed structure with some recently reported similar PCF-based devices in Table 2. As seen from this table, except for [18], our proposed structure has considerably higher sensitivity than the values in these works. It must be noted that although the case of [18] has higher wavelength sensitivity, it has lower amplitude sensitivity than our work.

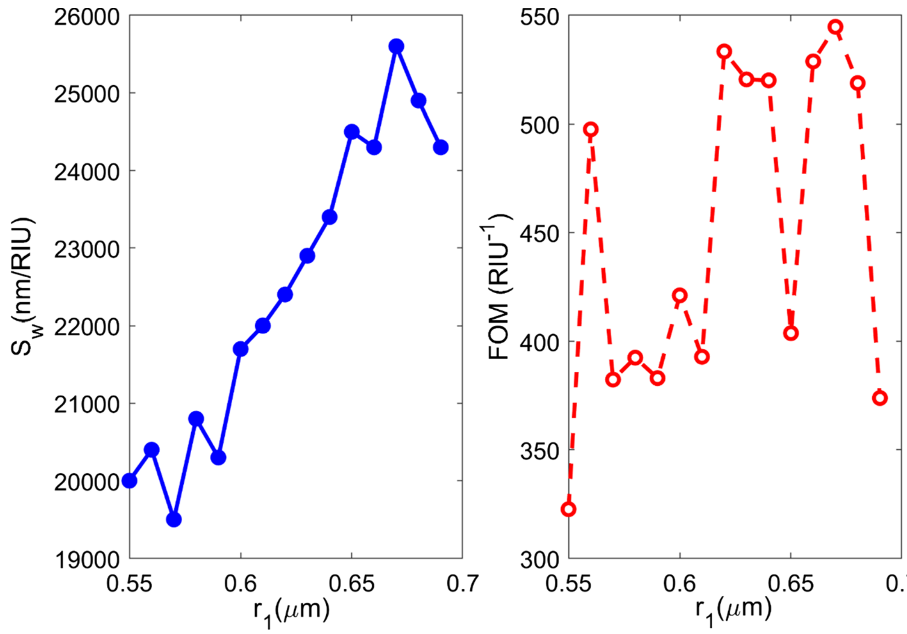

Fig. 6 Calculated wavelength sensitivity (left) and FOM (right) for different first ring air hole radii

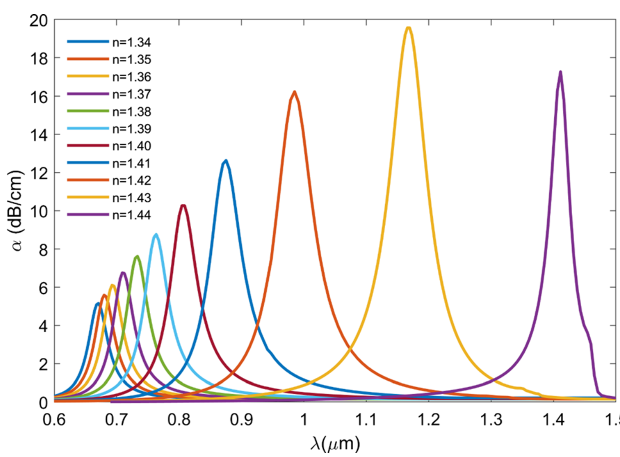

Fig. 7 Confinement loss spectra for analyte RI varying from 1.34 to 1.44

We hope that our proposed PCF sensor has taken a step forward for increased sensitivity by using four open rings instead of covering the entire fiber surface with gold and TiO_2 layers.

5 Conclusions

In this paper, we investigate a novel PCF-SPR sensor design with four open-ring channels for an analyte RI range between 1.34 and 1.44. The sensing performance of the proposed sensor is analyzed numerically by the FDTD method. The sensor characteristics of the proposed structure are investigated versus the geometrical parameters of the fiber and plasmonic material. The simulation results show maximum wavelength and amplitude sensitivity of 25,600 (nm/RIU) and 7367 RIU^{-1}, respectively, with a low propagation loss. Also, the highest figure of merit (FOM) as 547 RIU^{-1} is achieved for the analyte RI of 1.43. The presence of a TiO_2 layer under the plasmonic layer leads to enhanced sensing characteristics. Our results demonstrate better performance characteristics than several reported similar works. Because of the low loss and high wavelength and amplitude sensitivity, the proposed sensor is a promising candidate for application in medical diagnosis, detecting various bio-samples in the lab-on-fiber platform and environmental monitoring.

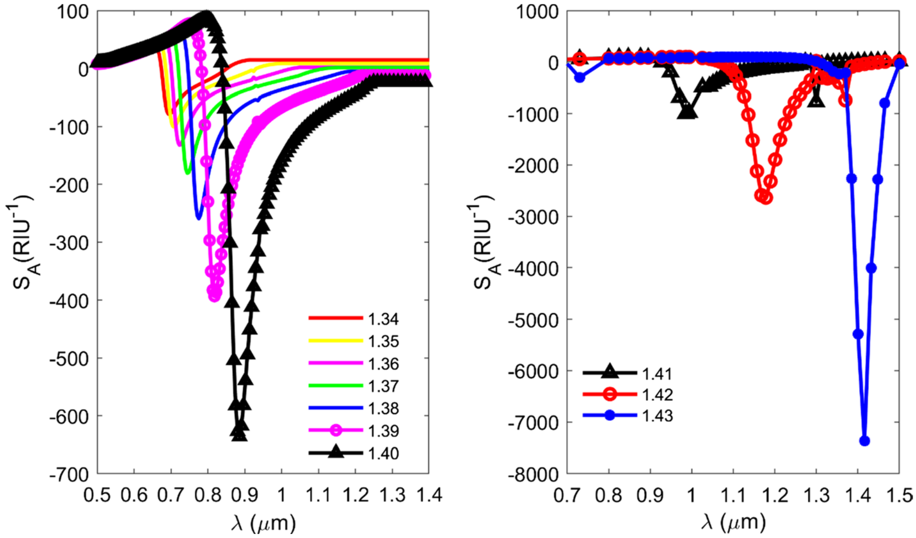

Fig. 8 Amplitude sensitivity of the proposed sensor with optimized parameters (left) RI = 1.34–1.40, (right) RI = 1.41–1.43

Table 1 Performance of the proposed sensor for an analyte RI detection range of 1.34 to 1.44

$\Delta\ n_a$(RIU)	S_W(nm/RIU)	$S_A\left(RIU^{-1}\right)$	FOM $\left(RIU^{-1}\right)$
1.34–1.35	1000	68.74	20.70
1.35–1.36	1000	100.2	21.39
1.36–1.37	2000	131.6	41.24
1.37–1.38	2000	181	39.34
1.38–1.39	3000	254	59.38
1.39–1.40	4000	393.1	73.07
1.40–1.41	7000	636.2	106.83
1.41–1.42	11,000	1001	152.77
1.42–1.43	18,000	2636	230.32
1.43–1.44	25,600	7367	547

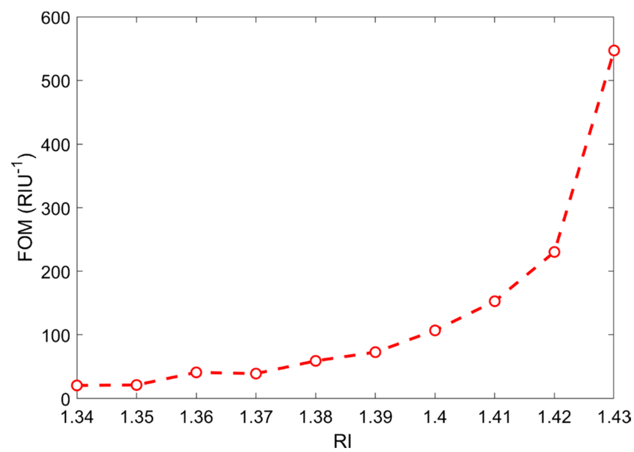

Fig. 9 FOM values of the proposed sensor for different analyte refractive indices

Table 2 Comparison of sensing characteristics of the proposed sensor with similar recent works

Structure	RI range	Max wavelength sensitivity (nm/RIU)	Max amplitude sensitivity (RIU^{-1})	FOM (RIU^{-1})	References
Ex-centric PCF	1.33–1.40	14,200	7428	141	[28]
PCF sensor	1.33–1.41	18,000	2843	400	[29]
D-shaped open channel	1.33–144	x-pol 17,000 y-pol 16,000	603.7 432.19	320 283.33	[30]
Dual-core open channel	1.33–1.45	38,000	1286	760	[18]
PCF sensor with four open surface rings	1.34–1.44	25,600	7367	547	Our work

Funding The authors declare that no funds, grants, or other support were received during the preparation of this manuscript.

Data availability The data sets generated during the current study are not publicly available but are available from the corresponding author on reasonable request.

Declarations

Conflict of interest The authors have no relevant financial or non-financial interests to disclose.

References

1. Sharma, A.K., Pandey, A.K., Kaur, B.A.: Review of advancements (2007–2017) in plasmonics- based optical fiber sensors. Opt. Fiber Technol. **43**, 20–34 (2018)
2. Azman, M.F., Mahdirazi, G.A., Wong, W.R., Aoni, R.A., Adikan, F.M.R.: Design and fabrication of copper-filled photonic crystal fiber based polarization filters. Appl. Opt. **58**, 2068–2075 (2019)
3. Zao, L., Han, H., Lian, Y., Luan, N., Liu, J.: Theoretical analysis of all-solid D-type photonic crystal fiber based plasmonic sensor for refractive index and temperature sensing. Opt. Fiber Technol. **50**, 165–171 (2019)
4. Momota, M.R., Hasan, M.R.: Hollow-core silver coated photonic crystal fiber plasmonic sensor. Opt. Mater. **76**, 287–294 (2018)
5. Meshginqalam, B., Barvestani, J.: Performance Enhancement of SPR Biosensor Based on Phosphorene and Transition Metal Dichalcogenides for Sensing DNA Hybridization. IEEE Sens. J. **18**(18), 7537 (2018)
6. Khanikar, T., Singh, V.K.: Gold grating assisted SPR based D-shaped single mode fiber for detection of liquid refractive index. Opt. Quant. Electron. **51**, 296 (2019)
7. Arasu, P.T., Noor, A.S.M., Shabaneh, A.A., Yaacob, M.H., Lim, H.N., Mahdi, M.A.: Fiber Bragg grating assisted surface plasmon resonance sensor with graphene oxide sensing layer. Opt. Commun. **380**, 260–266 (2016)
8. Liu, Q.H., Yan, B., Liu, J.J.: U-shaped photonic quasi-crystal fiber sensor with high sensitivity based on surface plasmon resonance. Appl Phys Express. **12**(5), 052014 (2019)
9. Hasan, M.R., Akter, S., Rifat, A.A., Rana, S., Ali, S.A.: Highly sensitive gold-coated photonic crystal fiber biosensor based on surface Plasmon resonance. Photonics **4**, 18 (2017)
10. Wang, X.X., Zhu, J.K., Wen, X.L., Wu, X.X., Wu, Y., Su, Y.W., Tong, H., Qi, Y.P., Yang, H.: Wide range refractive index sensor based on a coupled structure of Au nanocubes and Au film. Opt. Mater. Express **9**(7), 3079–3088 (2019)
11. Piliarik, M., Vaisocheroá, H., Homola, J.: A new surface plasmon resonance sensor for high-throughput screening applications. Biosens. Bioelectron. **20**(10), 2104–2110 (2005)
12. An, G.W., Li, S.G., Yan, X., Zhang, X.N., Yuan, Z.Y., Wang, H.Y., Zhang, Y.N., Hao, X.P., Shao, Y.N., Han, Z.C.: Extra-broad photonic crystal fiber refractive index sensor based on surface plasmon resonance. Plasmonics **12**(2), 465–471 (2017)
13. Paul, A.K., Sarkar, A.K., Khaleque, A.: Dual-core photonic crystal fiber plasmonic refractive index sensor: A numerical analysis. Photonic Sens. **9**(2), 151–161 (2019)
14. Tong, K., Wang, F.C., Wang, M.T., Dang, P., Wang, Y.X., Sun, J.R.: D-Shaped photonic crystal fiber biosensor based on silver-graphene. Optik **168**, 467–474 (2018)
15. Dash, J.N., Jha, R.: Highly sensitive D shaped PCF sensor based on SPR for near IR. Opt. Quant. Electron. **48**(2), 137 (2016)
16. Hautakorpi, M., Mattinen, M., Ludvigsen, H.: Surface plasmon resonance sensor based on three hole microstructured optical fiber. Opt. Express **16**(12), 8427–8432 (2008)
17. Momtaj, M., Mou, J.R., Kamrunnahar, Q.M., Islam, Md.A.: Open-channel-based dual-core D-shaped photonic crystal fiber plasmonic biosensor. Appl. Opt. **59**(29), 8856–8865 (2020)
18. Sakib, N., Hassan, W., Kamrunnahar, Q.M., Momtaj, M., Rahman, T.: Dual core four open channel circularly slotted gold coated plasmonic biosensor. Opt. Mater. Express **11**(2), 273–288 (2021)
19. Zha, F.N., Li, J.S., Sun, P.J., Ma, H.J.: Highly sensitive selectively coated D-shape photonic crystal fibers for surface plasmon resonance sensing. Phys. Lett. A **383**(15), 1825–1830 (2019)
20. Liu, E.X., Tan, W., Yan, B., Xie, J.L., Ge, R., Liu, J.J.: Robust transmission of orbital angular momentum mode based on a dual-cladding photonic quasi-crystal fiber. J. Phys. D Appl. Phys. **52**, 325110 (2019)
21. Mahfuz, M.A., Hasan, M.R., Momato, M.R., Masud, A., Akter, S.: Asymmetrical photonic crystal fiber based plasmonic sensor using the lower birefringence peak method. OSA Continuum **2**, 1713–1725 (2019)
22. Luan, N., Wang, R., Lv, W., Yao, J.: Surface plasmon resonance sensor based on D-shaped microstructured optical fiber with hollow core. Opt. Express. **23**, 8576–8582 (2015)
23. Haque, E., Hossain, M.A., Namihira, Y., Ahmed, F.: Microchannel based plasmonic refractive index sensor for low refractive index detection. Appl. Opt. **58**(6), 1547–1554 (2019)
24. Chao, L., Jianwei, W., Xin, J., Famei, W., Lin, Y., Jingwei, L., Guanglai, F., Xianli, L., Qiang, L., Tao, S., Chu, P.K.: Near–infrared surface plasmon resonance sensor based on photonic crystal fiber with big open rings. Optik. **207**, 164466 (2020)
25. Mahfuz, M.A., Hossain, M.A., Hague, E., Hai, N.H., Namihira, Y., Ahmed, F.: A bimetallic-coated, low propagation loss, photonic crystal fiber based plasmonic refractive index Sensor. Sensors. **19**, 3794 (2019)
26. Gupta, B.D., Verma, R.K.: Surface plasmon resonance-based fiber optic sensors: Principle, probe designs, and some applications. J. Sens. **2009**, 979761 (2009)
27. Meshginqalam, B., Barvestani, J.: Comparative study of the highly sensitive plasmonic sensor based on a D-Shaped photonic crystal fiber with silver or gold layers. Phys. Scr. **96**, 125535 (2021)
28. Liu, C., Fua, G., Wanga, F., Yib, Z., Xua, C., Yanga, L., Liua, Q., Liua, W., Lia, X., Mua, H., Sunc, T., Chud, P.K.: Ex-centric core photonic crystal fiber sensor with gold nanowires based on surface plasmon resonance. Optik. **196**, 163173 (2019)
29. Haider, F., Ahmmed, R., Ahmed, R., Miroshnichenko, A.E.: Highly amplitude-sensitive photonic crystal- fiber-based plasmonic sensor. J. Opt. Soc. Am. B. **35**, 11 (2018)
30. Momtaj, M., Mou, J.R., Kamrunnahar, Q.M., Islam, Md.A.: Open-channel-based dual-core D-shaped photonic crystal fiber plasmonic biosensor. Appl. Opt. **59**, 29 (2020)